Adsorption, Desorption, and Reaction of a Gallium Nitride Precursor, $(H_2GaNHNMe_2)_2$, on HfO_2

Bing Luo, Sung Yong Lee, and J. M. White*

Department of Chemistry and Biochemistry, Center for Materials Chemistry, The University of Texas at Austin, Austin, Texas 78712

Received July 3, 2003. Revised Manuscript Received November 25, 2003

The adsorption, desorption, and reaction of a dimeric gallium nitride precursor, $(H_2GaNHNMe_2)_2$, on amorphous HfO_2 are studied using TPD, AES, isothermal reaction spectroscopy (IRS), and temperature-programmed reaction (TPR). When dosed below 120 K, $(H_2GaNHNMe_2)_2$ adsorbs and desorbs molecularly and TPD results are consistent with a phase-transition model involving a low-temperature phase (phase A) that transforms irreversibly, between 190 and 215 K in competition with desorption, to a slightly more stable phase (B). The IRS, TPR, and AES data show that the dimers dissociate to monomers during dosing at 355 K, that GaN starts to form at 550 K, and that film-forming reactions become fast at 575 K. The results are consistent with monomer N−N bond cleavage to form hydrides, H_2GaNH and HGaNH, that eliminate hydrogen to produce GaN. The GaN films are examined using X-ray diffraction (XRD) and scanning electron microscopy (SEM).

1. Introduction

Chemical vapor deposition (CVD) of gallium nitride has attracted extensive interest because of its applications in high-power, high-efficiency optoelectronic devices.[1] High-quality films were obtained, typically on Al_2O_3(0001) substrates, using tri-organyl gallium and ammonia as the precursors,[1−3] but high-deposition temperatures were required and dealing with carbon contamination was challenging.[4] New precursors, particularly those containing direct gallium−nitrogen bonds, have been studied to address these problems.[4−11] Hydride derivatives including H_3Ga(quinuclidine),[12] $(H_2GaNH_2)_3$,[5] and $(H_2GaN_3)_n$[9] are a group of attractive precursors that do not contain any Ga−C bonds and produced GaAs and GaN at much lower temperatures. On the other hand, alternative nitrogen sources were investigated to replace ammonia.[13−17] 1,1-Dimethylhydrazine, H_2NNMe_2, was found to decompose at much lower temperatures than ammonia, and GaN films were prepared at lower temperatures.[15−17]

Combining these two types of advantages, a dimeric gallium compound containing both hydrido and hydrazido ligands, 1,1-dimethylhydrazidogallane, $(H_2GaNHNMe_2)_2$, was synthesized and characterized.[18] This compound exhibits remarkable room-temperature stability and volatility compared to most of the gallium hydride compounds. Previous studies showed that it decomposed to gallium metal when heated in a sealed glass capillary or in a hot-wall, low-pressure CVD reactor.[18] To explore its utility as a precursor for growing gallium-containing films we investigate its adsorption and desorption properties and pyrolysis on a supported inert oxide film, HfO_2, which is compatible with the heating and cooling methods used in ultrahigh vacuum (UHV) surface science, in particular, temperature-programmed desorption (TPD), temperature-programmed reaction (TPR), and isothermal reaction spectroscopy (IRS) using a time-of-flight mass spectrometer (TOF-MS)[19−21] and a line-of-sight dosing system

* Corresponding author. Fax: 512-471-9495. E-mail: jmwhite@mail.utexas.edu.

(1) Stringfellow, G. B. *Organometallic Vapor-Phase Epitaxy*: *Theory and Practice, 2nd ed.*: Academic Press: New York, 1999.
(2) Amano, H.; Sawaki, N.; Akasaki, I.; Toyoda, Y. *Appl. Phys. Lett.* **1986**, *48*, 353−355.
(3) Morkoc, H.; Mohammad, S. N. *Science* **1995**, *267*, 51−55.
(4) Neumayer, D. A.; Ekerdt, J. G. *Chem. Mater.* **1996**, *8*, 9−25.
(5) (a) Hwang, J.-W.; Hanson, S. A.; Britton, D.; Evans, J. F.; Jensen, K. F.; Gladfelter, W. L. *Chem. Mater.* **1990**, *2*, 342−343. (b) Hwang, J.-W.; Campbell, J. P.; Kozubowski, J.; Hanson, S. A.; Evans, J. F.; Gladfelter, W. L. *Chem. Mater.* **1995**, *7*, 517−525.
(6) Lakhotia, V.; Neumayer, D. A.; Cowley, A. H.; Jones, R. A.; Ekerdt, J. G. *Chem. Mater.* **1995**, *7*, 546−552.
(7) Miehr, A.; Ambacher, O.; Rieger, W.; Metzger, T.; Born, E.; Fischer, R. A. *Chem. Vap. Deposition* **1996**, *2*, 51.
(8) Park, H. S.; Waezsada, S. D.; Cowley, A. H.; Roesky, H. W. *Chem. Mater.* **1998**, *10*, 2251−2257.
(9) McMurran, J.; Kouvetakis, J.; Smith, D. J. *Appl. Phys. Lett.* **1999**, 74, 883−885.
(10) Devi, A.; Rogge, W.; Wohlfart, A.; Hipler, F.; Becker, H. W.; Fisher, R. A. *Chem. Vap. Deposition* **2000**, *6*, 245−252.
(11) Sung, M. M.; Kim, C.; Yoo, S. H.; Kim, C. G.; Kim, Y. *Chem. Vap. Deposition* **2002**, *8*, 50−52.
(12) Foord, J. S.; Whitaker, T. J.; O'Hare, D.; Jones, A. C. *J. Cryst. Growth* **1994**, *136*, 127−132.
(13) Gaskill, D. K.; Bottka, N.; Lin, M. C. *J. Crystal Growth* **1986**, *77*, 418−423.
(14) Friedman, D. J.; Norman, A. G.; Geisz, J. F.; Kurtz, S. R. *J. Cryst. Growth* **2000**, *208*, 11−17.
(15) Lee, R. T.; Stringfellow, G. B. *J. Electron. Mater.* **1999**, *28*, 963−969.
(16) Bourret-Courchesne, E.; Ye, Q.; Peters, D. W.; Arnold, J.; Ahmed, M.; Irvine, S. J. C.; Kanjolia, R.; Smith, L. M.; Rushworth, S. A. *J. Cryst. Growth* **2000**, *217*, 47−54.
(17) Hsu, Y. S.; Hong, L. S.; Huang, K. F.; Tsay, J. E. *Thin Solid Films* **2002**, *419*, 33−39.
(18) Luo, B.; Gladfelter, W. L. *J. Chem. Soc., Chem. Commun.* **2000**, 825−826.
(19) Kim, C.; Yan, X.-M.; White, J. M. *Rev. Sci. Instrum.* **2000**, *71*, 3502−3505.
(20) Yan, X.-M.; Kim, C.; White, J. M. *J. Vac. Sci. Technol. A* **2001**, *19*, 2629−2635.
(21) Lee, S. Y.; Luo, B.; Sun, Y.-M.; White, J. M.; Kim, Y. *Appl. Surf. Sci.* **2004**, *222*, 234−242.

10.1021/cm034583y CCC: $27.50
Published on Web 01/21/2004

complemented with Auger electron spectroscopy (AES). Use of the UHV techniques minimizes the pre- and post-deposition gas-phase reactions allowing a direct probe to surface reactions. These in-situ surface science studies and ex-situ characterization of the films are reported in this paper.

2. Experimental Section

UHV System, Precursor, and Substrate. The UHV system, as previously described,[21] was designed for studying surface chemistry of large molecules. We highlight two features here: a differentially pumped TOF-MS with a cryogenically cooled copper tube at the entrance for the suppression of background signals, and a line-of-sight dosing system.[21,22] In this study, the system was modified by adding a turbomolecular pump on the main chamber. On the basis of Ar-dosing tests, the pumping speed was constant over the range of pressures used in our experiments. The typical base pressure was 5.0×10^{-10} Torr.

The synthesis and characterization of the precursor, $(H_2GaNHNMe_2)_2$, were previously reported.[18] In this study, the precursor was further purified by sublimation at 45 °C into a precursor vessel maintained at 0 °C and frequently pumped with a turbomolecular pump. This operation removed trace impurities possibly present after the sublimation on a standard Schlenck line, and the precursor was stored for several months under vacuum at room temperature. The room-temperature vapor pressure of this precursor was ca. 0.4 Torr, as measured by connecting the precursor vessel to a capacitance pressure gauge.

The substrate was a smooth, amorphous HfO_2 film (thickness, ca. 40 nm) on a nickel foil prepared by physical vapor deposition (PVD).[23,24] Tungsten wires and an alumel−chromel thermal couple were spot-welded onto the back of the sample and this assembly was mounted through tantalum claps onto a Cu sample holder. The resulting assembly could be reproducibly and controllably cooled by liquid N_2 to 100 K or resistively heated to 1100 K. The sample was cleaned via repeated Ar^+ sputtering and annealing to 1000 K. Several such 1.0×1.0 cm^2 substrates were used in this study. As noted above, choice of the HfO_2/Ni substrate, rather than a single crystal sapphire, was based on our previous experience with it, its inertness to the precursor, and the ease of controlled temperature programming. Sapphire substrates, usually heated with a resistive heater or electron bombardment, are difficult to achieve precisely controlled temperatures on the surface of interest. As expected, the HfO_2 substrate shows a minimum reactivity in this study; for example, after several TPD experiments without sputtering or annealing, the surface contamination is limited to a few atom % of C and N (refer to Figure 7b below) and no Ga signal accumulates. These concentrations are not reduced by heating to 1000 K. We speculate that some defects acting as active sites react with a small amount of dose to form surface carbide and nitride species, and no further reaction occurs after these limited reactions.

Temperature-Programmed Desorption (TPD). The precursor was stored in a glass vessel and an ion gauge monitored the pressure of the dosing line. The precursor was maintained at 298.0 ± 0.1 K, and the dosing line was maintained at a slightly higher temperature (300−305 K). Before each dose, the precursor was degassed for 5 min and the ion gauge indicated a constant pressure (1.8×10^{-5} Torr). The flux onto the substrate from the line-of-sight dosing was approximately 10× that obtained by backfilling. Calculations based on the chamber pressures were not used to determine the relative dose because, as described below, a significant amount of H_2NNMe_2 was present and increased during the dose, likely the result of decomposition of $(H_2GaNHNMe_2)_2$ in the dosing line and on surfaces within the chamber. It is known that the precursor begins to decompose at temperatures above 360 K.[18] The spectra of all ions up to 500 amu were collected at a rate of two spectra per second, and, except when indicated otherwise, all the TPDs were conducted at a heating rate of 2.0 K/s.

Isothermal Reaction Spectroscopy (IRS). To examine steady-state kinetics, isothermal reaction spectra were measured while dosing a constant flux of the precursor. With the substrate temperature fixed between 300 and 700 K, 1−500 amu spectra were gathered before, during, and after dosing. For these experiments the precursor source was maintained at 309.0 ± 0.1 K, and the dosing line was maintained at slightly higher temperatures (310−315 K). Before each dosing, the ion gauge on the dosing line indicated a constant pressure of 5.0×10^{-5} Torr. During dosing, the chamber pressures were typically $2.5-3.2 \times 10^{-7}$ Torr. After each run, the substrate was cleaned by sputter−anneal cycles followed by AES to verify the cleanliness. Under conditions where GaN formed, IRS data were gathered on both the clean and GaN-covered surfaces.

Temperature-Programmed Reactions (TPR). Deepened reaction path insight was obtained by complementing IRS results with temperature-programmed reaction (TPR) data. In these experiments, the HfO_2 substrate was heated from 280 to 800 K at 0.8 K/s. At 300 K, a constant dose of $(H_2GaNHNMe_2)_2$ was initiated. TOF-MS signals were collected through the whole heating range. The precursor was maintained at 308.0 ± 0.1 K, and the ion gauge of the dosing line indicated 4.1×10^{-5} Torr prior to the dosing. During dosing the chamber pressure was $2.2-2.3 \times 10^{-7}$ Torr. For comparison, dimethylhydrazine, H_2NNMe_2, TPR data were gathered using the same procedure with a heating rate of 1.0 K/s. The chamber pressure was 7.0×10^{-8} Torr during the dosing. A baseline TPR experiment with no dose was also conducted.

GaN Film Depositions on HfO_2 and Al_2O_3(0001). With the same dosing conditions as in the TPD experiments, depositions were conducted for 40 min on HfO_2 at 650 and 750 K, and Al_2O_3(0001) at 750 K. During the depositions, the chamber pressure was $1.0-1.2 \times 10^{-7}$ Torr. The 1.0×1.0 cm^2 Al_2O_3(0001) substrate was polished on one side. To improve heating, a 200-nm Ta film was deposited by PVD on the unpolished side. The sample was clamped onto a thin (0.15 mm) Ta plate that was mounted onto the electrical joints through spot-welded W wires. The temperature was measured with an IR thermometer.

Auger Spectroscopy (AES), Scanning Electron Microscopy (SEM), and X-ray Diffraction (XRD) Measurements. AES data were gathered in-situ using a single-pass cylindrical mirror electron energy analyzer. SEM images of the GaN films were obtained ex-situ on a LEO 1530 scanning electron spectrometer with a 5-kV accelerating voltage and an X-ray fluorescence (EDS) detector. The XRD patterns were recorded on a Bruker AXS D8 Advance diffractometer using a copper anode. To intensify the diffractions from the films and diminish the diffractions from the substrates, a modified grazing incidence method was employed in which the X-ray incidence angle was chosen at 8° and the detector behind a collimator block with Soller slits scanned 2θ angles up to 80°.

3. Results

Temperature-Programmed Desorption of $(H_2GaNHNMe_2)_2$. Keeping in mind that gallium has two isotopes, ^{69}Ga and ^{71}Ga, a systematic evaluation reveals that molecular $(H_2GaNHNMe_2)_2$ desorption dominates the TPD spectra and only 15 ions of differing atomic composition exhibit peaks above background for a 60-s dose at 100 K (see Supporting Information). There are no desorption peaks above 250 K. The TPD peaks for gallium-containing ions (masses ≥ 69 amu) and mass

(22) Chan, A. S. Y.; Skegg, M. P.; Jones, R. G. *J. Vac. Sci. Technol. A* **2001**, *19*, 2007−2012.
(23) Park, H. J.; Sun, Y.-M.; Troiani, H.; Santiago, P.; Yacaman, M. J.; White, J. M. *Surf. Sci.* **2002**, *521*, 1−9.
(24) Yan, X.-M.; Ni, J.; Robbins, M.; Park, H.; Zhao, W.; White, J. M. *J. Nanopart. Res.* **2002**, 525−533.

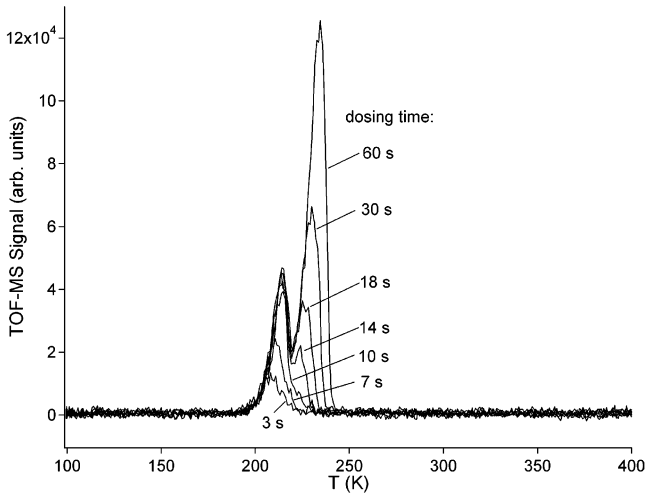

Figure 1. TPD spectra of $H_2GaNHNMe_2$ at a heating rate of 2.0 K/s. The substrate was held at 100 K while dosing a constant flux for the indicated time.

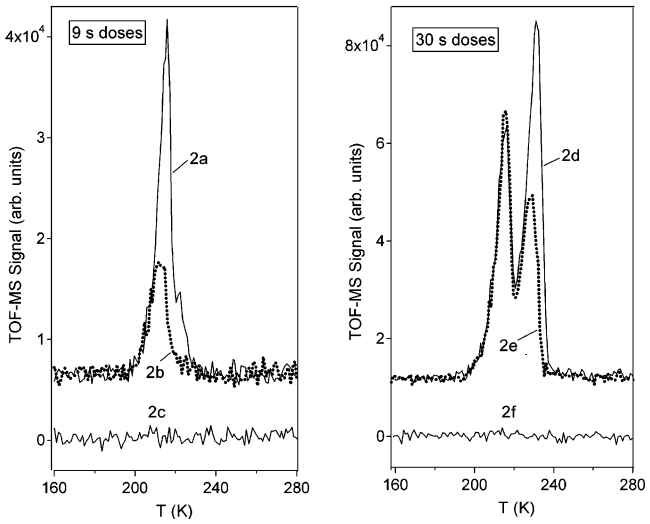

Figure 2. Comparison of $H_2GaNHNMe_2$ TPD spectra, with and without annealing, of 9-s (left side) and 30-s (right side) doses of $(H_2GaNHNMe_2)$ at 100 K: a and d, no annealing; b and e annealing at 190 K for 30 min; c and f, annealing at 210 K for 10 min. After annealing the sample was cooled to 150 K before initiating TPD.

46 amu ($Me_2NH_2^+$) are located at the same temperatures as those for the parent ion $(H_2GaNHNMe_2)_2^+$ (mass 262 amu), indicating that these are part of the fragmentation pattern of $(H_2GaNHNMe_2)_2$. Two exceptions are $HGa(NHNMe_2)_2^+$ (188 amu) and $[HGa(NHNMe_2)_2 - Me]^+$ (173 amu), which may be generated from electron-induced reactions (see below). The monomer ion, $H_2GaNHNMe_2^+$ (mass 130 amu), exhibits the highest intensity and Figure 1 shows how, for a substrate at 100 K, its profile for a series of doses varies.

For doses up to 10 s there is one desorption peak. For doses of 14 s or more the low-temperature peak (215 K) saturates, and a second, higher-temperature peak (224 K) emerges. This peak intensifies without limit and the peak temperature moves slowly higher with increasing dose, reaching 236 K for a 60-s dose. For both peaks, the leading edges align, and, for the higher temperature peak, the peak position and very sharp decay are typical of zero-order kinetics. This behavior continues for even higher doses (not shown).

In general, TPD probes absorbate/substrate and adsorbate/adsorbate physical and chemical interactions. For molecular adsorption and desorption,[25−28] when an adsorbate interacts strongly with the substrate, submonolayers and monolayers desorb at higher temperatures than multilayers, and in most cases, the monolayer desorption peaks saturate for high exposures. When the adsorbate/adsorbate interaction dominates, typically only one desorption peak is observed for all doses from submonolayers to multilayers. The TPD characteristics in Figure 1 are unusual and suggest a relatively unique adsorption and desorption process that we characterize in more detail below. Before doing so, other features of the TPD are noted. For small ions (masses ≤ 60 amu excluding mass 46 amu), in addition to the peaks tracking the 262 amu signal, an additional peak at 193 K appears. This peak is attributed to dimethylhydrazine, H_2NNMe_2, desorption. As mentioned, a significant amount of H_2NNMe_2 was present in the UHV chamber during dosing and some was adsorbed on the substrate and its surroundings. Because the liquid-N_2-cooled shield at the entrance of the TOF-MS did not fully trap the H_2NNMe_2 molecules coming from directions other than the substrate, the molecular H_2NNMe_2 desorption peak includes contributions from the surroundings as well as the substrate. However, after analyzing a variety of TPD results, including those shown below, we conclude the adsorbed H_2NNMe_2 does not affect in a detectable manner the TPD characteristics of $(H_2GaNHNMe_2)_2$.

To characterize the striking behavior illustrated in Figure 1, we dosed $(H_2GaNHNMe_2)_2$ for either 9 or 30 s at 100 K, annealed at selected temperatures for selected times, recooled, and then gathered and compared TPD spectra (Figure 2). Without annealing, only the low-temperature peak is present in the TPD of the 9-s dose (Figure 2 trace a), whereas both peaks appear for the 30-s dose (Figure 2 trace d). Annealing at 190 K for 30 min or 210 K for 10 min removes some (Figure 2 traces b and e) or all of the adsorbate (Figure 2 traces c and f). Considering that a higher-temperature peak reflects a more stable adsorption state, it is striking that, for the 30-s dose, annealing at 190 K removes intensity from the higher-, not the lower-, temperature peak (Figure 2 trace e). Confirming that small amounts of H_2NNMe_2 do not alter $(H_2GaNHNMe_2)_2$ desorption, there is some H_2NNMe_2 desorption at 193 K in Figure 2 trace d but not trace e (not shown).

The TPD spectra of Figures 1 and 2 suggest that the two desorption peaks represent two different, likely nonequilibrium, phases of $(H_2GaNHNMe_2)_2$, denoted A and B, rather than monolayer and multilayer adsorption. As a working hypothesis, we suppose that for doses at 100 K only phase A forms, and during TPD (or annealing) phase B does not form at a measurable rate until the temperature reaches some point between 205 and 210 K (see below). According to this model, anneal-

(25) Sun, Y.-M.; Sloan, D. W.; McEllistrem, M.; Schwaner, A. L.; White, J. M. *J. Vac. Sci. Technol. A* **1995**, *13*, 1455−1460.
(26) Sloan D.; Sun, Y.-M.; Ihm, H., White, J. M. *J. Phys. Chem. B* **1998**, *102*, 6825−6830.
(27) Nishimura, S. Y.; Gibbons, R. F.; Tro, N. J. *J. Phys. Chem. B* **1998**, *102*, 6831−6834.
(28) Aubuchon, C. M.; Davison, B. S.; Nishimura, A. M.; Tro, N. J. *J. Phys. Chem.* **1994**, *98*, 240−244.

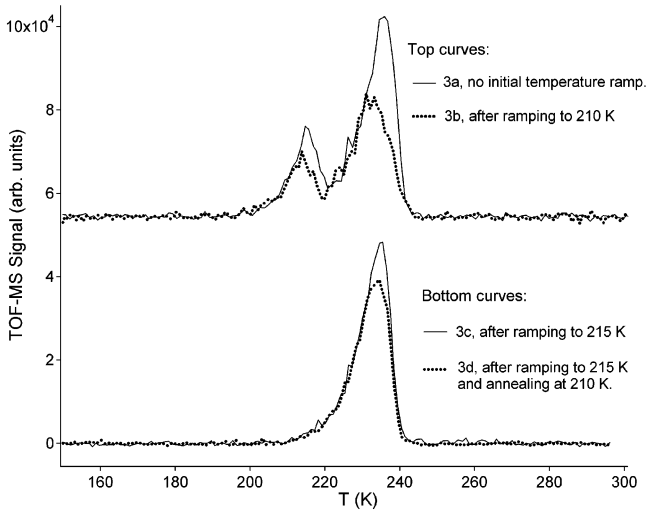

Figure 3. TPD spectra of $H_2GaNHNMe_2$ after thermal processing to indicated temperatures and cooling to 150 K. All doses are 60 s.

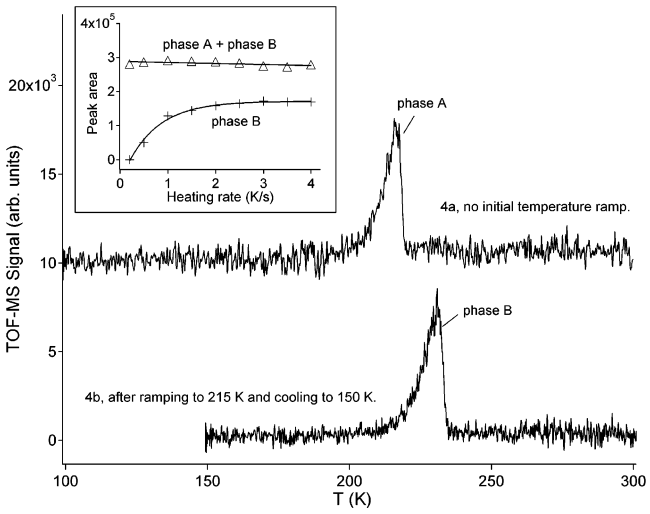

Figure 4. TPD spectra of $H_2GaNHNMe_2$ at a heating rate of 0.2 K/s for 60-s doses at 100 K: (a) with no initial temperature ramp and (b) after ramping to 215 K and cooling to 150 K. For the same doses but varying heating rates, the inset plots the total amount desorbed (phase A + phase B) and the amount desorbed at a higher temperature (phase B).

ing at 190 K removes considerable adsorbate by desorption of A, but no B forms. During the subsequent TPD, desorption of A commences at the expected temperature and with the expected intensity but is sluggish enough to allow the temperature (increasing at 2.0 K/s) to reach that where transformation of A to B is competitive with desorption from A.

To further test the phase-transition postulate, 60-s doses at 100 K were ramped (2.0 K/s) to selected temperatures and rapidly cooled to 150 K prior to gathering TPD data. Compared to the TPD without an initial thermal excursion (Figure 3a), ramping to 205 K does nothing (not shown), whereas ramping to 210 K indicates desorption of A and relatively slow conversion of A to B such that, in TPD after rapid cooling to 150 K, the desorption of A remains relatively intense (Figure 3b). After ramping to 215 K, no low-temperature intensity remains but the higher-temperature-peak intensity is preserved (Figure 3c). Finally, after ramping to 215 K, cooling to 210 K, and holding there for 10 min before cooling to take TPD, the profile, Figure 3d, exhibits no A intensity but the B peak remains strong. In other experiments (not shown), after ramping to 215 K, the system was annealed for extended periods at temperatures up to 205 K. In these cases, the profile of Figure 3c was reproduced with no loss of intensity.

These results are consistent with the proposed model—ramping to 210 K leads to desorption of some A and, only above 210 K, to irreversible conversion of A to B. Once conversion to B is complete, subsequent annealing at any $T \leq 205$ K neither desorbs B nor converts B to A. On the other hand, annealing at 210 K slowly desorbs B.

We next examined the influence of the heating rate on TPD profiles measured after 60-s doses at 100 K (Figure 4 and Supporting Information). For TPD without any preliminary thermal processing, only A desorbs when the ramp rate is 0.2 K/s (Figure 4a), but both A and B desorb when the rate is 2 K/s (Figure 1). When the dose is processed by heating to 215 K and recooling, only B appears when the TPD ramp rate is 0.2 K/s (Figure 4b). The inset of Figure 4 shows that, without preliminary thermal processing, the total amount desorbed (A + B) does not vary strongly with heating rate but the amount appearing in B increases with heating rate and approaching an asymptote that is about 0.7 of the total. Consistent with the proposed model, these results indicate that for the coverage formed by a 60-s dose at 100 K, there is enough time between 190 and 210 K for all the $(H_2GaNHNMe_2)_2$ to desorb before reaching the temperature required to convert A to B when the heating rate is 0.2 K/s. For ramp rates from 0.5 to 2.0 K/s, the amount of B desorbing increases because 210 K is reached before all the A desorbs. For ramp rates between 2 and 4 K/s, the amount of B desorbed no longer increases measurably with ramp rate. While the time interval required to cover the temperature interval between the onset of desorption of A and the onset of conversion to B is steadily shortened, if the time interval is short enough, most of the A that desorbs does so within a very narrow time/temperature interval that overlaps with the temperature where A transforms rapidly to B. Under these circumstances, conversion from A to B is accompanied by a "pulse" of A with intensity that does not vary significantly with heating rate.

For shorter (25 s) doses, we examined how varying the substrate temperature (100−215 K) during dosing impacts subsequent TPD taken upward from the dosing temperature (Figure 5). There is no intensity in state B for dosing temperatures below 140 K. As the dosing temperature moves from 140 to 190 K, intensity shifts from A to B with no change in total intensity. Above 190 K, the total intensity drops, and the fraction desorbed as A also decreases and drops to zero at 210 K. For doses at 215 K, nothing adsorbs.

IRS of $(H_2GaNHNMe_2)_2$ on HfO_2. We turn to IRS of $(H_2GaNHNMe_2)_2$ on HfO_2. In the experiments, the substrate temperature was fixed (300−700 K) and the TOF-MS intensities were monitored as a function of time before, during (80 s), and after dosing a constant flux of the precursor. Over the 1−500 amu range recorded, only a few signals rise above background. Three of particular interest (Figure 6) are (H_2GaNH-

Table 1. Intensity of Selected Ions during Isothermal Reaction

	temperature (K)									
ion	300	350	400	450	500	550	580	600	650	700
$(H_2GaNHNMe_2)_2^+$ (262 amu)	1.0	1.0	0.74	0.65	0.48	0.34	0.26	0.13	0	0
$(H_2GaNHNMe_2)^+$ (130 amu)	1.0	1.0	1.0	0.87	0.78	0.68	0.59	0.24	0.14	0.05
$(H_2GaNHNMe_2GaH_2)^+$ (203 amu)	1.0	1.0	1.0	0.85	0.75	0.65	0.56	0.22	0	0
$HGa(NHNMe_2)_2^+$ (188 amu)	1.0	1.0	1.0	0.90	0.78	0.63	0.52	0.20	0	0
Ga^+ (69 amu)	1.0	1.0	1.0	0.90	0.81	0.66	0.57	0.25	0.12	0.07
H_2^+ (2 amu)	1.0	0.93	0.90	0.95	1.1	1.1	2.0	1.9	2.5	3.4

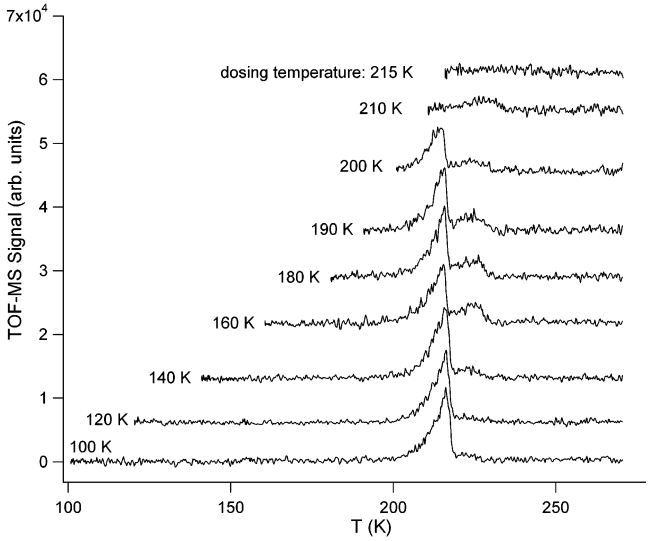

Figure 5. Ramped at 0.4 K/s starting at the indicated dosing temperature, TPD of $H_2GaNHNMe_2$ for 25-s doses.

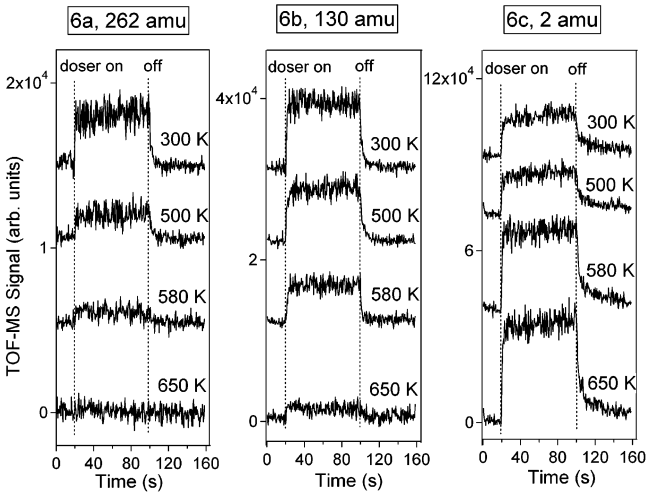

Figure 6. Selected isothermal reaction spectra (IRS) of $(H_2GaNHNMe_2)_2^+$ (262 amu), $(H_2GaNHNMe_2)^+$ (130 amu), and H_2^+ (2 amu) during dosing of $(H_2GaNHNMe_2)_2$ on HfO_2 held at the indicated temperatures. In each case, dosing commenced at 20 s and terminated at 100 s.

$NMe_2)_2^+$, $H_2GaNHNMe_2^+$, and H_2^+ (262, 130, and 2 amu, respectively). Each of these, as well as all others that respond, rise promptly, maintain nearly steady intensities, and decay promptly when the dose is terminated.

Normalized to unity at 300 K (Table 1), the steady-state H_2^+ intensity increases with temperature above 550 K accompanied by loss of 262 and 130 amu intensity. More significantly, the intensity ratio, I_{262}/I_{130}, drops as the temperature rises; I_{262} goes to zero at 600 K, about 100 K before I_{130} does. We conclude that dimer dissociation to monomer becomes important at high temperatures and, further, that reaction, consuming both monomer and dimer and releasing H_2, becomes important for $T > 550$ K. Significantly, *the same temperature variation was found when dosing on either clean HfO_2 or the as-formed film surface.*

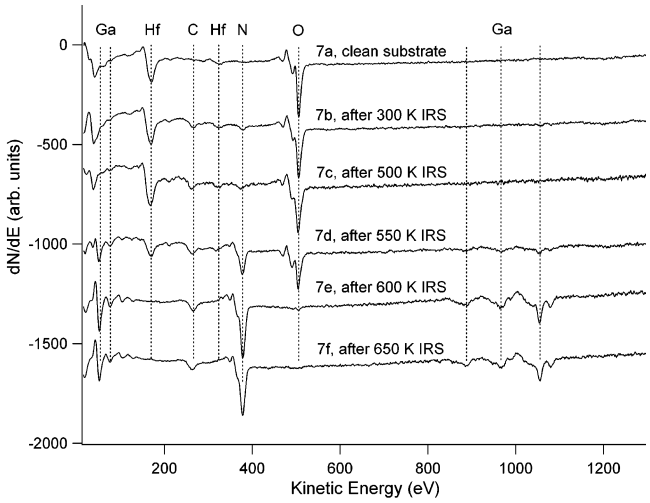

Figure 7. AES for the initial HfO_2 surface (top curve) and after the 80-s isothermal reactions described in Figure 6.

In each IRS experiment the background intensity of H_2NNMe_2 constantly increases, reflecting a relatively slow pumping speed mainly due to its relatively strong physisorption and slow release from nonsample surfaces. The intensities of $H_2NNMe_2^+$ and smaller fragment ions of H_2NNMe_2 often reach 15× the intensities of the Ga-containing ions, making it very difficult to track reactions on the growing film surface. Clearer pictures for these small species were obtained from TPR experiments described below.

AES, Figure 7, provides complementary information for the 80-s doses of Figure 6. Only Hf and O appear before the precursor is dosed (trace 7a). After dosing at and below 500 K (traces 7b and 7c) there is a small amount of C (ca. 10 atomic %) and N (ca. 3 atomic %) but no Ga. These amounts of C and N were also found in AES taken after TPD. Dosing at 550 K (trace 7d) leads to Ga and increased N signals, and at and above 600 K (traces 7e and 7f) the N and Ga intensities reach constant values and the O and Hf signals disappear. Importantly, *the C signal does not vary significantly with the dose temperature between 500 and 650 K.*

Taken together, the IRS and AES data indicate the following: (1) below 350 K, there is no surface reaction; (2) between 350 and 400 K, dimer dissociates to monomer, and monomer desorbs, but no surface species accumulate; (3) as the temperature increases the desorbed dimer intensity drops faster than that of the monomer; and (4) at and above 550 K, a GaN film forms that incorporates very little carbon.

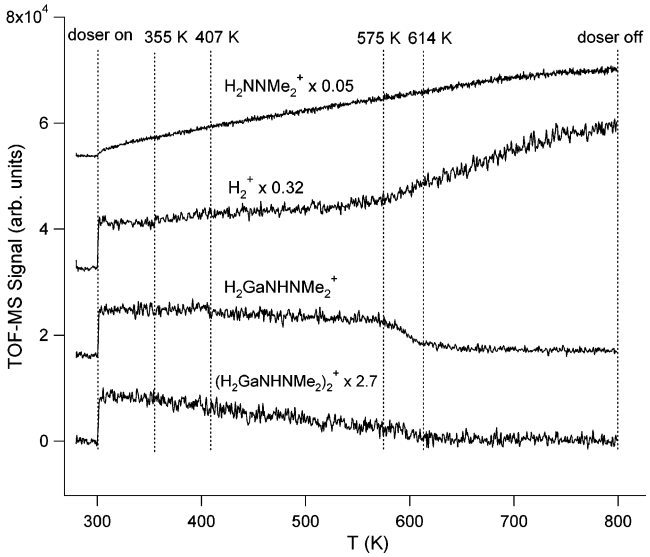

Figure 8. Temperature-programmed reaction (TPR) spectra of $(H_2GaNHNMe_2)_2^+$, $H_2GaNHNMe_2^+$, H_2^+, and $H_2NNMe_2^+$ for $(H_2GaNHNMe_2)_2$ dosed on HfO_2. The ramp (0.8 K/s) was initiated at 280 K, and $(H_2GaNHNMe_2)_2$ dosing began as the temperature reached 300 K. Dosing terminated when the temperature reached 800 K.

TPR of $(H_2GaNHNMe_2)_2$ on HfO_2. To complement IRS and to help identify reaction paths, we gathered temperature-programmed reaction data. In these experiments, TOF-MS data were recorded as the substrate temperature was ramped, and at 300 K the doser was opened to deliver a constant flux of $(H_2GaNHNMe_2)_2$. Four scaled profiles, dimer $(H_2GaNHNMe_2)_2^+$, monomer $H_2GaNHNMe_2^+$, H_2^+, and $H_2NNMe_2^+$ are plotted in Figure 8. The dimer signal is constant from 300 to 355 K, gradually decreases above 355 K, and becomes zero above ca. 610 K. The monomer intensities are constant from 300 to ca. 407 K, decrease slowly from 407 to 575 K, decrease quickly from 575 to 614 K, and approach zero above 614 K. Other signals (not shown) trace the monomer (203, 188, 158, 115, and 69 amu) or dimer profile (218 amu).

For ions smaller than 60 amu, the signals are normalized to the 60 amu ($H_2NNMe_2^+$) intensity at 300 K (Figure 9). All these ion intensities rise in concert with 60 amu and, except for 27 and 28 amu, grow with the same temperature dependence up to about 575 K. The scaled 27 and 28 amu signals lie slightly above the 60 amu curve between 300 and 500 K due to background effects including CO desorption involving nonsample surfaces. Above 575 K, the signals separate by varying amounts. Other small mass ion signals (see Supporting Information) follow one of the profiles of Figure 9. Specifically, 59 amu follows 60 amu (H_2NNMe_2); 42, 39, 17, 16, 15, and 14 amu follow 43 amu; 40 follows 41 amu; 46 and 18 amu follow 45 amu; and 29 amu follows 30 amu.

These results indicate, consistent with AES and IRS, that reactions to form films occur at and above 575 K and that increased ion signals below that temperature are the result of a growing background pressure of dimethylhydrazine, H_2NNMe_2. This is traceable to the unavoidable dosing of this species along with the nitride precursor.

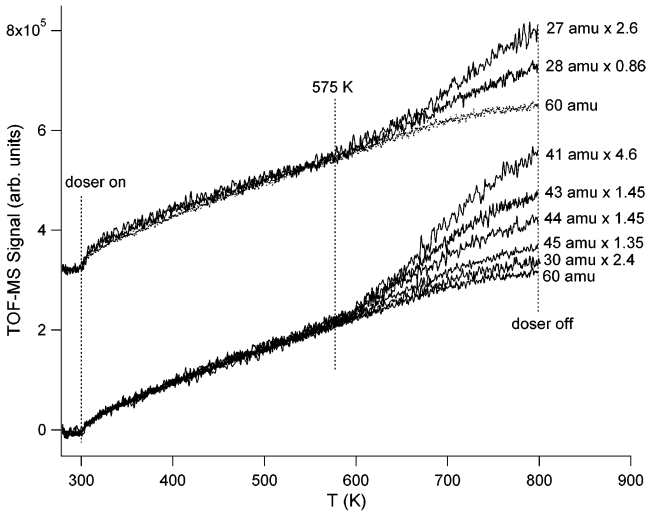

Figure 9. TPR spectra of low amu species obtained during dosing of $(H_2GaNHNMe_2)_2$ on HfO_2. The ramp (0.8 K/s) was initiated at 280 K, and $(H_2GaNHNMe_2)_2$ dosing began as the temperature reached 300 K. Dosing terminated when the temperature reached 800 K.

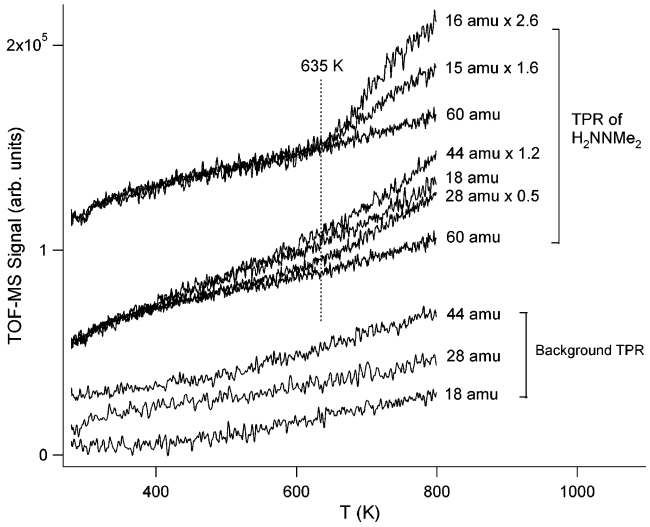

Figure 10. TPR spectra taken during dosing of H_2NNMe_2 on HfO_2 (upper seven curves) and TPR of background (lower three curves). The ramp (1.0 K/s) was initiated at 280 K, and $(H_2GaNHNMe_2)_2$ dosing began as the temperature reached 300 K. Dosing terminated when the temperature reached 800 K.

For comparison, TPR experiments (Figure 10) were done by dosing H_2NNMe_2 in the absence of $(H_2GaNHNMe_2)_2$. The 60 amu ($H_2NNMe_2^+$) signal rises steadily as when $(H_2GaNHNMe_2)_2$ is dosed. A 5-fold reduction of the dosing rate does not alter this trend. Except for 15 and 16 amu, other fragments of H_2NNMe_2 faithfully track the 60 amu signal (not shown). The 15 and 16 amu signals track 60 amu from 280 to 635 K, but rise faster above 635 K. The 44, 28, and 18 amu signals split away from the 60 amu signal at as low as 400 K. Confirmed by heating in the absence of dosing H_2NNMe_2 (bottom of Figure 10), the behavior of these ions is attributed to desorption of CO, CO_2, and H_2O from nonsample surfaces that warm slowly during the temperature ramp. Over the 1−500 amu range, signals other than 18, 28, and 44 amu remained constant at background levels during temperature ramping in the absence of a dose.

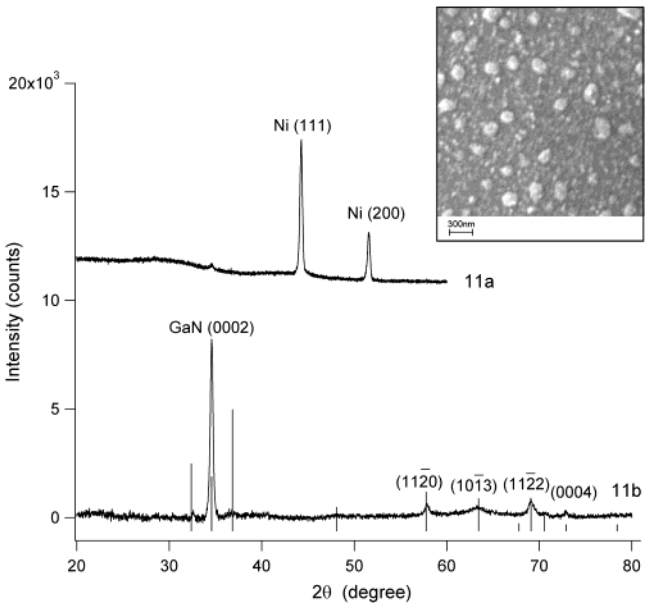

Figure 11. XRD patterns collected via a detector scan with a fixed incidence angle of 8° for (a) GaN film formed by dosing at 650 K for 40 min on a HfO_2 film covering a Ni foil and (b) GaN film deposited at 750 K for 40 min on $Al_2O_3(0001)$. The thin vertical lines represent the standard hexagonal GaN diffractions. The inset is an SEM image of the sample used in (a).

In the upper half of Figure 10, the higher intensities of masses 15 and 16 amu above 635 K indicate decomposition of H_2NNMe_2. Bourret-Courchesne et al reported that H_2NNMe_2 decomposed in a hydrogen atmosphere with the first step being the cleavage of the N−N bond at 593 K to form NH_2 and NMe_2, and further decomposition of NMe_2 started at 788 K.[16] Our results are qualitatively consistent with their proposal, i.e., the higher intensities of masses 16 and 15 amu above 635 K could arise from NH_2 and CH_3 species formed by pyrolysis of H_2NNMe_2 to break the weak N−N bond.

SEM, EDS, and XRD Characterization of Films. For a GaN film deposited on HfO_2 at 650 K for 40 min, the in-situ AES measurements indicate 10 atomic % C, 40% N, and 50% Ga averaged over the AES sampling depth (ca. 6 nm). The SEM image (inset of Figure 11) comprises a range of nanoscale particles. This morphology is not surprising considering the substrate is an amorphous film HfO_2, and crystalline GaN films are usually grown on crystalline $Al_2O_3(0001)$ substrates.[2,3] To compare with AES, energy-dispersive spectrometric (EDS) analyses at several spots give an average composition of 50 atomic % N, 44% Ga, 4% C, and 2% O. The oxygen is the result of the requisite through-air transfer. The larger amount of carbon found in AES is taken as indicating that its concentration in the bulk of the film probed by EDS is much lower than its surface concentration, probed by both EDS and AES. For both EDS and AES, the calculated percentages of Ga and N are not inconsistent with stoichiometric GaN. Standardization would be required for quantitation.

Consistent with the SEM observation, XRD shows amorphous character (Figure 11a) in which, besides the strong Ni signal from the metal that supports the HfO_2 substrate, only a weak peak is found at $2\theta = 34.6°$. The XRD patterns of films deposited at 750−800 K are essentially the same as those in Figure 11a, showing that only amorphous GaN can be grown in this temperature range. To pursue the formation of crystalline GaN, a film was deposited on $Al_2O_3(0001)$ at 750 K. The XRD pattern (Figure 11b) exhibits diffraction features characteristic of polycrystalline hexagonal GaN. Because a grazing incidence angle was used, substrate Al_2O_3 diffraction peaks are not observed. Moreover, recalling that the data were collected with a fixed X-ray incidence angle of 8°, the intense GaN(0002) diffraction indicates a preferred orientation roughly (with a 9° deviation) along the *z*-axis of the $Al_2O_3(0001)$ substrate. This result is consistent with growth of GaN, not Ga metal, on HfO_2. More work is needed to characterize film growth on $Al_2O_3(0001)$.

Scheme 1

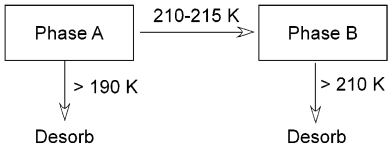

4. Discussion

Structural Transformation Model. The TPD characteristics (Figure 1) are atypical in the sense that low doses form adsorbate structures that desorb at higher temperatures than the multilayers that form during high doses.[25−28] For $(H_2GaNHNMe_2)_2$ dosed at 100 K on amorphous HfO_2, just the opposite occurs.

Keeping in mind that there is no dissociative adsorption and that the relatively low desorption temperature requires a weakly bound adsorbate, we propose, on the basis of all the TPD data, that a kinetically controlled, irreversible phase transition occurs in competition with desorption (Scheme 1). This model possesses the following features: (1) $(H_2GaNHNMe_2)_2$ forms a metastable phase (A) on the HfO_2 surface for doses at and below 120 K; (2) in TPD, phase A starts to desorb at 190 K generating the low-temperature peak, and at slightly higher temperatures, sluggishly and irreversibly rearranges to form phase (B) that desorbs at slightly higher temperatures; (3) compared to desorption, the phase-change kinetics are much slower below 210 K and significantly faster above 210 K; and (4) phase B desorption is detectable at 210 K.

Scheme 1 is consistent with the observation that, for a 2.0 K/s temperature ramp, the low-temperature peak saturates above a minimum coverage and, for higher coverages, there is an unsaturable higher temperature peak. During the 10 s required to pass from 190 to 210 K, zero-order desorption from multilayers of phase A will occur at the same rate provided the exposed adsorbate−surface area is independent of the dose. Scheme 1 is also consistent with heating rate variations (Figure 4). If the heating rate is below 0.2 K/s, at least 100 s is required to pass from 190 to 210 K and during this time the desorption rate overwhelms the rate of transforming phase A to B so only the lower temperature desorption peak appears. As the heating rate increases, less than 100 s is required and more adsorbates survive to higher temperatures where conversion to B becomes fast. The effects of annealing at 190 K before TPD (Figure 2) are readily understood. While annealing at 190 K desorbs some phase A, there is no

Scheme 2

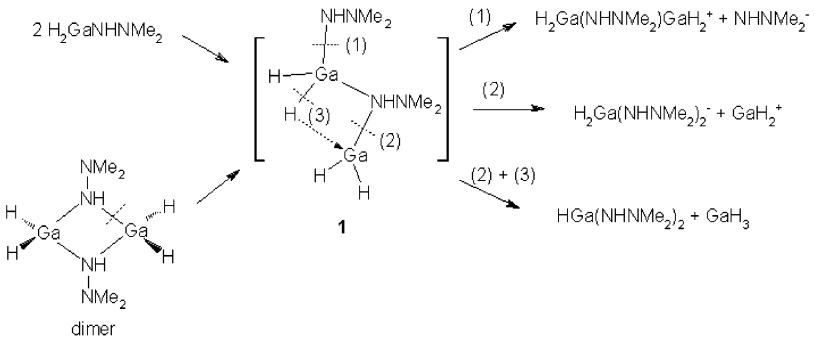

conversion from A to B at this temperature so in subsequent TPD the phase A intensity does not change. Because desorption of B is slow at 210 K (Figure 3 trace 3d), the fact that all molecules desorb during annealing at 210 K indicates that the rate of transforming A to B at this temperature is slow compared to the rate of desorption of A. Further, the sluggish phase transition below 210 K is evidenced by the incomplete phase transition after a rapid heating to 210 K (Figure 3 trace 3b). The absence of phase A after heating to 215 K (Figure 3 trace 3c) indicates that the A-to-B transition is complete at this temperature. The irreversibility of the A-to-B transformation is clearly indicated by the inability to transform any B into A for conditions where large amounts of B and negligible amounts of A are prepared (Figure 3 traces 3c and 3d).

To account for the effects of dosing temperature on the population of phase B, Scheme 1 must be modified slightly. After dosing at 140 K or higher, heating at 0.4 K/s leads to population of B whereas dosing the same amount at lower temperatures does not. For these conditions, the phase B peaks are not simply the result of thermal activation during the ramp because the time required to pass from 140 K to the desorption temperature is certainly shorter than the time required to pass from 100 K to the desorption temperature. We ascribe the population in B to its formation during adsorption. Whereas, for substrate temperatures lower than 140 K, inbound adsorbates at 300 K are rapidly and structurally quenched and remain in phase A, but when dosed above 140 K, some B forms locally during the quenching process.

Although the proposed phase-transition model accounts for all the TPD results, the structures of these phases remain unresolved. We presume that phase A is amorphous and phase B is ordered and involves intermolecular hydrogen bonding similar to that observed in the crystalline solid-state structure of $(H_2GaNHNMe_2)_2$.[18]

For low doses (3, 7, and 10 s) (Figure 1), phase A dominates desorption, and the leading edges overlap consistent with zero-order desorption kinetics. However, the absence of very sharp trailing edges is taken as a reflection of the mixing in of some phase B desorption. When only phase A is present (Figure 4a) zero-order desorption characteristics are clearly observed. Leading-edge kinetic analysis[28,29] yields a desorption activation energy of 71 ± 3 kJ/mol for phase A.

For the higher-temperature phase B, zero-order desorption characteristics are evident (Figures 1 and 4b). Compared to phase A, kinetic analysis gives a barely distinguishable, but slightly higher, desorption activation energy of 74 ± 1 kJ/mol for phase B.

Reactions of $(H_2GaNHNMe_2)_2$ on HfO_2. We now turn to consideration of the events leading to film growth during isothermal and temperature-programmed reaction (IRS and TPR). The former determines some general trends and the latter determines some important details. In this discussion we recall that a comparison of Figures 9 and 10 indicates that, while directly dosing some dimethylhydrazine, H_2NNMe_2, is unavoidable, and while its partial pressure rises during dosing, its reactions, if they occur at all, have negligible effects on film growth. During TPR at constant incident flux, changes indicating dimer dissociation set in at ca. 355 K, e.g.

$$(H_2GaNHNMe_2)_2 \rightarrow 2\ H_2GaNHNMe_2 \qquad (1)$$

The departure of the I_{130}/I_{262} ratio from its initial value of 2.7 toward higher values (Figure 8) is taken as evidence. That I_{130} is constant between 355 and 407 K is interpreted as the coincidental offsetting of two competing effects: the decreased contribution from ion source fragmentation of dimers and the increased intensity of monomer desorption. This is supported by the IRS data that exhibit the same steady-state I_{130} signal for all temperatures between 300 and 400 K (Table 1).

The I_{262} and I_{130} ratio interpretation is incomplete because some Ga-containing ions with masses > 130 amu (203, 188, and 173 amu) follow the I_{130}, not the I_{262}, profile. One speculative possibility is illustrated in Scheme 2 where a different dimeric intermediate **1** is formed from coordinatively unsaturated monomers at or just above the surface. Electron impact ionization of **1** could form species with the masses described above: $H_2Ga(NHNMe_2)GaH_2^+$ (203 amu), $H_2Ga(NHNMe_2)_2^-$, and $HGa(NHNMe_2)_2$ (188 amu). The as-formed H_3Ga or H_2Ga would immediately decompose to Ga metal,[30] contributing to the overall Ga^+ mass intensity (the Ga^+ signal tracks $H_2GaNHNMe_2^+$). The 173 amu species can arise from fragmentation of $HGa(NHNMe_2)_2$. Also shown in Scheme 2, species **1** could be generated from the stable dimer via breaking a Ga−N bond. This is consistent with the appearance of these species in the

(29) King, D. A.; Madey, T. E.; Yates, J. T., Jr. *J. Chem. Phys.* **1971**, *55*, 3247−3253.

(30) Pulham, C. R.; Downs, D. J.; Goode, M. J.; Rankin, D. W. H.; Robertson, H. E. *J. Am. Chem. Soc.* **1991**, *113*, 5149−5162.

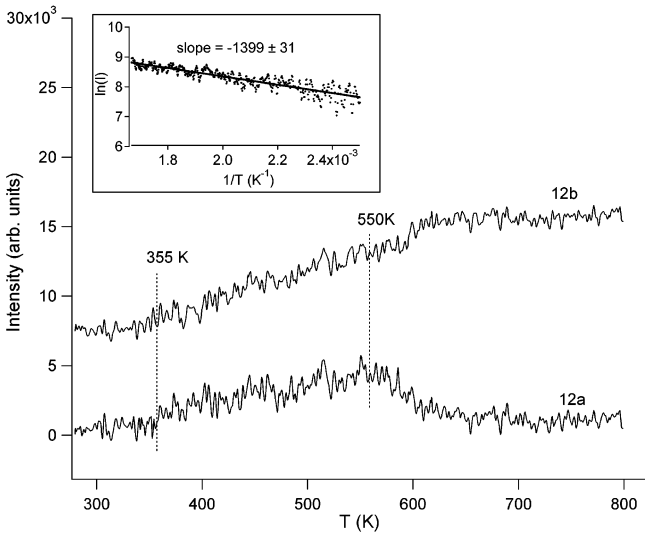

Figure 12. Calculated (see text) TPR profiles of *reacted* dimer (upper curve) and *desorbing* monomer (lower curve). The inset is the ln *I* vs 1/*T* plot for the reacted dimer, where the *I* and *T* data are obtained from Figure 12 (upper curve).

TPD, IRS, and TPR experiments at low temperatures where no surface reaction is evident. Ligand exchange reactions similar to that proposed in Scheme 2 for producing $HGa(NHNMe_2)_2$ and GaH_3 have been previously proposed for several solution-phase reactions involving gallium hydride compounds.[31,32] In TPR (Figure 8), the slight increase in the H_2^+ intensity starting at 355 K is attributable to increased desorption of monomer which has increased fragmentation to H_2^+ compared to that of the dimer. The formation of **1**, while plausible, remains speculative, especially on the surface.

Neglecting the plausible regeneration of dimers from **1**, the contribution of dimer fragmentation to the I_{130} signal can be subtracted from the total I_{130} signal to estimate the intensity attributable to monomer desorption (Figure 12a). Similarly, an estimate of the *reacted* dimer (due to all paths removing dimer signal) profile can be calculated by subtracting the measured I_{262} at any time from the initial dimer signal (Figure 12b). The temperature dependence of the monomer and reacted dimer intensities track each other up to 550 K, but above this temperature monomer desorption decreases while reacted dimer intensity continues to increase. The latter continues to 700 K where the dimer signal drops to zero (reacted percentage reaches 100%) and the monomer signal decays asymptotically to zero. Between 400 and 600 K, the *reacted* dimer intensity occurs with an effective activation energy of 11.6 ± 0.3 kJ/mol and according to our interpretation is dominated by the dimer-to-monomer dissociation energy (the inset of Figure 12).

The onset (355 K) of dimer-to-monomer dissociation lies very close to the temperature (363 K) at which gallium metal was observed in the decomposition of *bulk* $(H_2GaNHNMe_2)_2$.[18] We suggest that dimer-to-monomer dissociation initiates bulk decomposition, but, unlike surface decomposition, reactions such as the ligand exchange reactions (Scheme 2) occur with higher probability and can lead to metallic Ga by formation and decomposition of species such GaH_3. Under our vacuum conditions ligand exchange is less likely and other monomer decomposition paths dominate.

The AES measurements following isothermal reactions show Ga and N started to deposit at 550 K. Consistent with this, TPR experiments establish that monomer decomposition is facile at 575 K. After the TPR experiment a layer of material, presumably GaN, was found everywhere on the sample holder. That the $H_2NNMe_2^+$ intensity rises smoothly in passing through 575 K indicates that H_2NNMe_2 is not a major decomposition product. The relatively high intensities of 45 ($HNMe_2^+$) and 44 amu (NMe_2^+) compared to that of $H_2NNMe_2^+$ above 575 K (Figure 9) lead us to propose that the monomer, $H_2GaNHNMe_2$, decomposes via the cleavage of the N−N bond (Eqs 2 and 3, where (s) stands for a surface site). Because the 44 and 45 amu signals do not track each other above 575 K, more than one product is being desorbed. It is important to note that background contributions to 44 amu (Figure 10) are negligible compared with the intensities in Figure 9. We propose that adsorbed products of reactions 2 and 3, H_2GaNH and HGaNH, decompose to GaN and H_2 (Eqs 4 and 5). The production and desorption of H_2 is also clearly indicated in IRS (Figure 6c).

$$H_2GaNHNMe_2\,(s) \rightarrow H_2GaNH\,(s) + NMe_2\cdot \quad (2)$$

$$H_2GaNHNMe_2\,(s) \rightarrow HGaNH\,(s) + HNMe_2 \quad (3)$$

$$HGaNH\,(s) \rightarrow H_2 + GaN\,(s) \quad (4)$$

$$H_2GaNH\,(s) \rightarrow 3/2\ H_2 + GaN\,(s) \quad (5)$$

A detailed analysis (Figure 9 and plots in the Supporting Information) of ions from 40 to 46 amu supports the formation and desorption of dimethylamine $HNMe_2$, and the free radical NMe_2. Particularly important, a scaled version of 46 amu ($H_2NMe_2^+$, protonated dimethylamine) tracks the $HNMe_2^+$ signal. The 43, 42, and several other smaller ions had intensities higher than either 44 or 45 amu. This is taken as indicative of decomposing $HNMe_2$ and NMe_2 according to reactions such as those in eqs 6−8.

$$HNMe_2 \rightarrow H_2 + MeNCH_2\ (43\ amu) \quad (6)$$

$$Me_2N\cdot \rightarrow H\cdot + MeNCH_2 \quad (7)$$

$$MeNCH_2 \rightarrow H\cdot + MeNCH\cdot\ (42\ amu) \quad (8)$$

5. Conclusions

To describe the reversible adsorption and desorption of $(H_2GaNHNMe_2)_2$ on HfO_2, a model involving an irreversible phase transition occurring in competition with thermal desorption is proposed. This model accounts for the unusual TPD spectra in which a lower-temperature desorption grows, saturates, and is followed, for larger doses, by a higher-temperature unsaturable TPD peak. AES, IRS, and TPR spectra establish that the dimeric $(H_2GaNHNMe_2)_2$ begins to dissociate to form monomers at 355 K and the GaN starts to form at temperatures as low as 550 K with facile deposition at 575 K. The formation of GaN in this

(31) Jegier, J. A.; Mckernan, S.; Gladfelter, W. L. *Chem. Mater.* **1998**, *10*, 2041.
(32) Luo, B.; Young, V. G., Jr.; Gladfelter, W. L. *Inorg. Chem.* **2000**, *39*, 1705−1709.

study differs from that reported for bulk $(H_2GaNHNMe_2)_2$ samples in that the latter decomposed to Ga metal. This difference is attributed to differing monomer decomposition pathways. In UHV, we propose that the monomer decomposes via N−N bond cleavage, whereas for condensed phases ligand exchange to produce GaH_3 followed by Ga is more likely. SEM and XRD characterizations reveal the formation of amorphous GaN on HfO_2.

Acknowledgment. This work was supported by the Center for Materials Chemistry of the University of Texas at Austin and by the Robert A. Welch Foundation. We thank Dr. Hyun Jung Park and Mr. Qi Wang for their assistance in preparing the substrates, Prof. Wayne L. Gladfelter, Department of Chemistry, the University of Minnesota, for supplying a sample of the precursor, and Prof. Alan H. Cowley, Department of Chemistry and Biochemistry, the University of Texas at Austin, for his help in synthesizing additional precursor.

Supporting Information Available: Additional spectra obtained in the TPD experiments of $(H_2GaNHNMe_2)_2$ and TPR experiments of $(H_2GaNHNMe_2)_2$ and H_2NNMe_2 (pdf). This material is available free of charge via the Internet at http://pubs.acs.org.

CM034583Y